Accuracy Evaluation of Ultrawideband Time Domain Systems for Microwave Imaging

Accuracy Evaluation of Ultra-Wideband Time Domain Systems for Microwave Imaging

Xuezhi Zeng, *Student Member, IEEE,* Andreas Fhager,*Member, IEEE,* Mikael Persson, *Member, IEEE,* Peter Linner, *Life Senior Member, IEEE,* and Herbert Zirath, *Fellow, IEEE*

***Abstract*—We perform a theoretical analysis of the measurement accuracy of ultra-wideband time domain systems. The theory is tested on a specific ultra-wideband system and the analytical estimates of measurement uncertainty are in good agreements with those obtained by means of simulations. The influence of the antennas and propagation effects on the measurement accuracy of time domain near field microwave imaging systems is discussed. As an interesting application, the required measurement accuracy for a breast cancer detection system is estimated by studying the effect of noise on the image reconstructions. The results suggest that the effects of measurement errors on the reconstructed images are small when the amplitude uncertainty and phase uncertainty of measured data are less than 1.5 dB and 15 degrees, respectively.**

***Index Terms*—Biomedical Imaging, Measurement errors, Microwave imaging, Random noise, Time domain measurements.**

I. Introduction

As a potential imaging modality for biomedical applications, active microwave imaging has attracted considerable interest in the past few decades [1]–[4]. With active microwave imaging, biological tissues are classified based on their differences in dielectric properties. Several studies have shown that the variation is mainly due to different water content [5]–[8].

There are two main approaches to active microwave imaging: tomography and radar based imaging. Microwave tomography is a classic approach which leads to solving an inverse scattering problem. In a tomography system, an antenna array is used to transmit microwave signals into an object-under-test and receive scattered fields. By iteratively comparing the measured data with numerically calculated data, the dielectric properties of the object under test can be quantitatively reconstructed. Microwave tomography reconstructions based on mono-frequency, multiple frequency or time domain data have been numerically and experimentally studied [9]–[14]. It has been shown that highly stable and high-resolution reconstructions can be achieved by the use of ultra-wideband (UWB) data [13]–[14].

In contrast to microwave tomography, radar based imaging avoids complex image reconstruction algorithms and has been extensively investigated for biomedical applications in the last few years, e.g, breast cancer detection [15]–[19]. In this approach, a UWB signal is used to illuminate an object, and the reflected signal is measured at numerous locations. The amplitude and time arrival information of the reflected signals is utilized to identify the presence and location of significant scatters. As a result, a qualitative image of the object under investigation is obtained.

Measurements for UWB microwave imaging are generally carried out either in the frequency domain with the help of a vector network analyzer (VNA) [13], [17], [18], or in the time domain using a sampling oscilloscope [12]. With the VNA, scattering parameters at a number of discrete frequencies are measured and then utilized to synthesize time domain signals. The sampling oscilloscope uses an equivalent time sampling technique which constructs a UWB signal based on measurements over several repetitive wave cycles. In contrast to the equivalent-time system, a time domain system capable of real-time data acquisition [19] was recently applied to UWB microwave imaging and with this system, the scattered signal is acquired from a single-shot measurement.

In comparison with frequency domain systems, time domain systems have the advantage of fast acquisition of UWB data, which makes them more attractive for UWB applications, such as medical imaging, see-through-wall imaging radar [20], and ground-penetrating radar [21]. However, time domain systems have lower signal-to-noise-ratios (SNRs), which may produce distortion to the images. This was noted in [19] for tumor detection in breast phantoms.

In order to design a suitable time domain system for UWB microwave imaging, we need quantify the required measurement accuracy and investigate the factors that affect the measurement accuracy. This paper is devoted to these issues and focuses on medical applications using the tomographic approach.

In this paper, we derive analytical estimates of the measurement uncertainty of time domain systems. In order to validate the analysis, we investigate a specific time domain system and compare the estimated uncertainties with simulated results. Furthermore, we discuss the effects of antennas and propagation on the measurement accuracy of time domain imaging systems.

The degree of measurement accuracy required for a microwave imaging system is dependent on the specific application. As an example, the effect of noise on the reconstruction quality of a high contrast breast model is numerically studied in order to estimate the required measurement accuracy.

This work was supported in part by the Swedish Agency for Innovation Systems within the Chalmers Antenna Systems VINN Excellence Centre and in part by the Swedish Foundation for Strategic Research within the Strategic Research Center Charmant. The computations were performed on C3SE computing resources.

X. Zeng, A. Fhager, and M. Persson are with the Department of Signals and Systems, Chalmers University of Technology, 412-96 Gothenburg, Sweden.

P. Linner and H. Zirath are with the Microwave Electronics Laboratory, Chalmers University of Technology, 412-96 Gothenburg, Sweden.

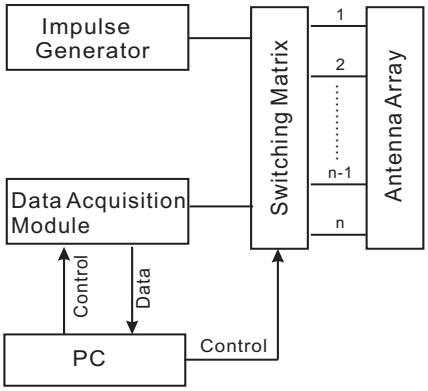

Fig. 1. Block diagram of a UWB time domain microwave imaging system.

II. UWB Time Domain System for Microwave Imaging

Fig. 1 shows the block diagram of a UWB time domain microwave imaging system. It consists of an impulse generator, a data acquisition module, an antenna array, a switching matrix and a personal computer (PC).

With this system, a UWB signal generated by the impulse generator is transmitted into an object under test and the scattered signal is received. This is performed for all the possible combinations of transmitting-receiving antenna pairs with the help of the switching matrix. The acquired signals are measured by means of the data acquisition module and the whole measurement is automated by using the PC.

Antennas in the microwave imaging system typically work in a range from hundred megahertz to several gigahertz and the choice of the frequency range is a tradeoff between the spatial resolution and penetration depth in materials of interest. Directional antennas are preferable in some cases in order to concentrate the radiated power in the imaging region.

In addition to the performance of the antennas, the tomographic approach imposes constraints on the properties of the antennas. The antennas need to be easily and accurately modeled in a electromagnetic computational solver. The antennas should also have small size in order to be configured in an antenna array. Monopoles are commonly used due to its simple structure [2]–[3], [13]. It has been shown that when placed in a lossy medium, the bandwidth of a monopole antenna increases significantly with the associated resistive loading. Our investigation is however general and not restricted to any specific type of antenna.

III. Measurement Uncertainty

The measurements are subject to errors that can be mainly classified into deterministic errors and random errors. Deterministic errors can be compensated for by using various calibration techniques [22]–[23]. We therefore only study the effects of random errors in the rest of the paper.

A. Random Error Analysis

The measurement of a time domain signal is affected by three different random error sources: thermal noise, quantization noise and time jitter [22]. The thermal noise and time jitter are nearly Gaussian and zero-mean random variables. The quantization noise is characterized by the least significant bit (LSB) and is uniformly distributed from -1/2 LSB to 1/2 LSB. We assume a noise free signal $x(t)$, then the jth sample of the real measured signal, y_j, can be expressed as follows:

$$y_j = x(T_j + \tau_j) + \varepsilon_j + \gamma_j, \tag{1}$$

where T_j is the target time of the jth sample, τ_j is the time jitter, ε_j is the thermal noise and γ_j is the quantization noise.

The variability of the time domain measurements is characterized by the standard deviation of several measurements carried out under repetitive conditions [24]:

$$\sigma_k(f) = \sqrt{\frac{1}{N}\sum_{i=1}^{N}(Y_{ik}(f) - \overline{Y_k(f)})^2} \tag{2}$$

Here N is the number of measurements, $Y_{ik}(f)$ is the fast Fourier transform (FFT) of the acquired measurement of index i. $\overline{Y_k(f)}$ is the average of the FFT of all measurements. $Y_{ik}(f)$ and $\overline{Y_k(f)}$ are either amplitude (in volts when k = 1) or phase (in degrees when k = 2).

As a result, $\sigma_1(f)$ and $\sigma_2(f)$ represent the uncertainties of spectral amplitudes and phases respectively. Defining $\text{SNR}(f) = \overline{Y_1(f)}/\sigma_1(f)$, the amplitude uncertainty is often expressed as a relative value in terms of SNR:

$$\sigma_{dB}(f) = 20\log_{10}[1 + 1/\text{SNR}(f)] \tag{3}$$

B. Analytical Estimates of Measurement Uncertainties

The amplitude and phase uncertainties defined by (2) and (3) can be estimated analytically based on the analysis presented below.

It is usually assumed that, after averaging, time jitter acts as a low pass filter [25]–[26]. Therefore, we can write:

$$\overline{Y_1(f)} \approx |X(f)| \cdot P(f), \tag{4}$$

where $X(f)$ is the frequency spectrum of the noise free signal $x(t)$ and $P(f)$ is the Fourier transform of the jitters probability density function. The latter can be expressed as [26]:

$$P(f) = e^{-0.5*(2\pi f\cdot\sigma_t)^2}, \tag{5}$$

where σ_t is the standard deviation of the time jitter in seconds. Therefore, the distorting effects of the jitter may be removed by means of deconvolution [25]–[26].

If the thermal noise and quantization noise are assumed to be white, noise will have a flat spectrum in the frequency domain. The standard deviation of spectral amplitude, $\sigma_1(f)$, can then be obtained from the following equation:

$$\sigma_1(f) = \sqrt{\frac{\sigma_Q^2}{f_s/2} + \frac{\sigma_T^2}{BW_N}} \cdot \sqrt{\frac{1}{N_{Avg}}} \tag{6}$$

Here $\sigma_Q^2 = \text{LSB}^2/12$ [27] and σ_T^2 are the quantization noise power and the thermal noise power, respectively. f_s is the sampling rate, BW_N is the effective noise bandwidth and N_{Avg} is the number of averages in the measurements.

Therefore, given a specified UWB time domain system, the SNR of a measurement can be estimated, based on (4) to (6).

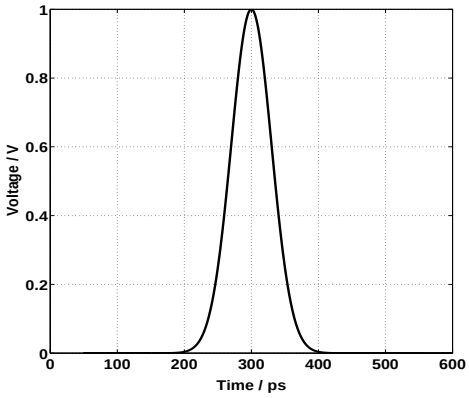

(a)

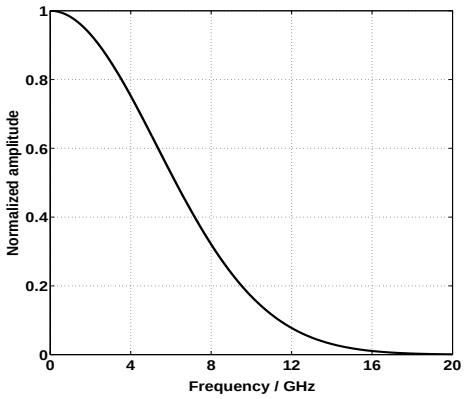

(b)

Fig. 2. The output signal of the impulse generator: (a) time domain waveform and (b) amplitude spectrum.

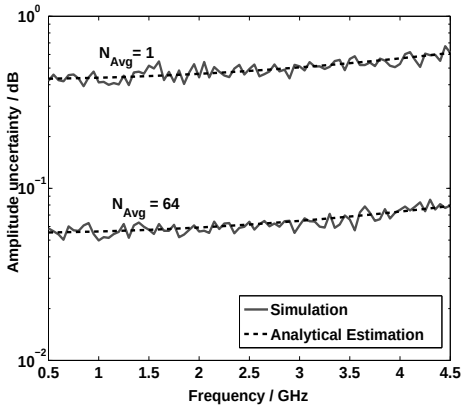

(a)

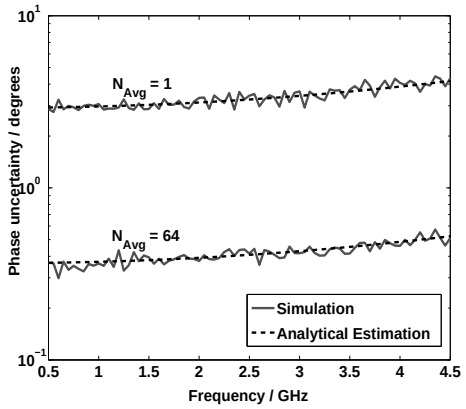

(b)

Fig. 3. Measurement uncertainties of (a) the spectral amplitudes and (b) the phases of a test signal.

Then the amplitude uncertainty can be obtained from (3). The phase uncertainty, $\sigma_2(f)$, is proportional to the relative error of the spectral amplitude and can be roughly estimated from the SNR [28]:

$$\sigma_2(f) \approx \arctan[1/\mathrm{SNR}(f)] \tag{7}$$

This equation gives the limit of the achievable phase measurement accuracy.

C. Comparison between Simulated Results and Analytical Estimates

Simulations can now be performed in order to validate the analysis above. In the simulations, we model the effects of random errors on a time domain measurement according to (1) and then calculate the amplitude and phase uncertainties from the simulated data. The obtained results are compared with the uncertainties estimated analytically by (4) – (7).

The specification data of an impulse generator in our lab [29] and a specific real time oscilloscope with bandwidth of 20 GHz and sampling rate of 80 Gsamples/s [30] are used for the simulations. The output voltage of the generator, $v(t)$, has a Gaussian shape with a full width half maximum duration of 70 picoseconds (ps). The time domain waveform and the normalized amplitude spectrum of the output are given in Fig. 2. The amplitude spectrum has a -3 dB bandwidth of around 4.5 GHz, which covers the frequency range of interest.

We disregard the antennas and propagation effects and assume that the received signals have the same waveform as the impulse signal $v(t)$. The received signals are then "measured" in the simulations with the time domain system and the measurement uncertainties are obtained from these simulations.

We take the maximum input of the oscilloscope as an example. The maximum input (the peak-to-peak amplitude) of the oscilloscope is $V_{p-p} = 8$ V and the corresponding thermal noise is $\sigma_T \approx 30$ mV RMS. We assume that the noise is bandlimited to the bandwidth of the oscilloscope, that is BW_N = 20 GHz. The LSB of the quantization is given by LSB = $V_{p-p}/2^n$, where $n = 8$ bits is the resolution of the oscilloscope. The quantization noise is frequency limited to half of the sampling frequency $f_s/2$ = 40 GHz. The time jitter is $\sigma_t \approx 1.6$ ps RMS, which is contributed by both the impulse generator and the oscilloscope. The thermal noise and time jitter are modeled as normally distributed random processes, and the modeled quantization noise has an uniform distribution.

Fig. 3 shows the amplitude and phase uncertainties obtained from the simulations in comparison with the theoretical estimates when the number of averages N_{Avg} = 1 and N_{Avg} =

64, respectively. The data is presented in a frequency range from 0.5 GHz to 4.5 GHz. The measurement uncertainties of the simulated measurement data are obtained from $N = 100$ repetitive waveforms.

The simulated results agree well with the theoretical estimates, which validates the analytical analysis. The results represent the highest accuracy can be achieved by using the investigated system for the specific simulated measurement.

D. Antennas and Propagation Effects

The antennas and propagation effects were neglected in the above simulation. In practical microwave imaging measurements, the antennas and signal propagation play important roles in determining the characteristic of the received signals.

First of all, an antenna works as a spatio-temporal filter, which makes the radiated signal distorted from the excitation signal. The same effect is present on the receiving side [31]. Furthermore, the signals received by different antennas vary in strength and the variation is dependent on the radiation pattern of the antennas, the size of the antenna array and the electrical properties of the imaging medium. Besides, different frequency components suffer different levels of attenuation and have different phase velocities (dispersion) in the propagation. In addition, due to multiple scattering effects, the signals acquired by the receiving antennas are superpositions of multi-path signals which have different strengths and arrival time.

Therefore, the received signals in the microwave imaging system are dependent on the antenna performance, the antenna array configuration and the electric properties of the imaging medium. If we denote the number of antenna elements by K and indicate the transmitting antenna with index 1, then the signal received by the antenna element with index k (k = 2, 3,.....K), $x_k(t)$, can be expressed as an inverse Fourier transform (IFFT):

$$x_k(t) = \text{IFFT}[V(f) \cdot T_k(f)] \tag{8}$$

Here $V(f)$ is the frequency spectrum of the generator output $v(t)$. $T_k(f)$ comprises the frequency response of the transmitting and receiving antennas and the propagation effects:

$$T_k(f) = \sum_{m=1}^{M_k} A_{km}(f) e^{j\theta_{km}(f)} \tag{9}$$

where M_k is the number of multi-path signals received by the antenna element with index k, $A_{km}(f)$ and $\theta_{km}(f)$ represent the amplitude and phase transfer functions respectively. The assumption we made about the antennas and propagation effects in the simulations corresponds to M_k = 1, $A_{km}(f) = A_k$, and $\theta_{km}(f) = B_k f$. Here both A_k and B_k are constants.

When dealing with far field problems, an analytical expression of $T_k(f)$ can be obtained, in which antennas are described by means of their impulse response [32]–[33]. However, we works on a near-field imaging approach and the complicated propagation environment makes it impractical to express $T_k(f)$ in an analytical way.

Instead, numerical simulations can be used to estimate $T_k(f)$ for a specific measurement configuration, from which the received signals can be obtained according to (8). Then by using the analytical estimates, we can evaluate the measurement uncertainties of time domain measurements. With the analytical analysis, we can also design a suitable system with given measurement accuracy.

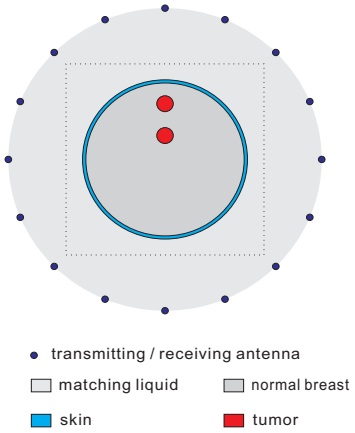

Fig. 4. Breast model and antenna array configuration used in the numerical studies.

IV. Effects of Noise on Image Reconstructions

Noisy measurements may degrade the image reconstruction quality. As a specific example, in this section we investigate the influence of noise on the reconstructions of a 2-D breast model by means of numerical simulations.

Breast cancer detection is one of the most researched applications of microwave imaging. Recently, it has been reported that the contrast in dielectric properties between the malignant tumor and normal breast tissue varies considerably depending on the compositions of the breast [8]. Our previous study showed that the sensitivity of image reconstructions to the measurement error is dependent on the dielectric contrast of the imaged object [34]. From the image reconstruction point of view, it is more challenging to handle high contrast objects, we therefore consider a high contrast breast model in this work.

Fig. 4 shows the breast model and the antenna array configuration used in the simulations. The model consists of a 2 mm skin layer, a circular healthy tissue with radius of 48 mm and two tumors with radius of 5 mm. The dielectric properties are assumed to be frequency independent and the permittivities and conductivities for skin, healthy tissue, and tumor are: ϵ_{skin} = 40, σ_{skin} = 1 S/m [7] ; ϵ_{breast} = 10, σ_{breast} = 0.2 S/m [8]; ϵ_{tumor}=55, σ_{tumor} = 1 S/m [8]. Sixteen antenna elements are equally spaced on a 19 cm diameter circle and immersed in a matching liquid with ϵ_{liquid} = 12 and σ_{liquid} = 0.2 S/m.

The measured scattering data was numerically generated by using a finite difference time domain (FDTD) program and totally 16×15 data sets were obtained. In the forward simulation, the grid cell size was 1 mm and the antennas were modeled as hard sources, which radiate electromagnetic energy by setting electric fields in FDTD grids. In numerical studies, the real antenna modeling gives the same quality reconstructions as those obtained based on hard source models as long as the antennas have the required bandwidths.

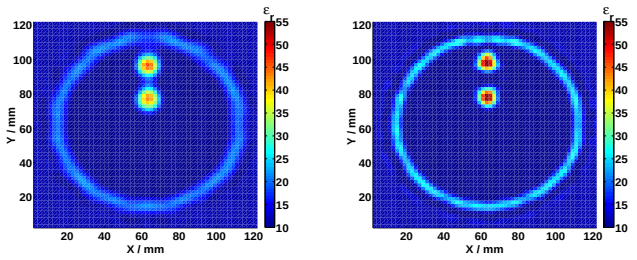

Fig. 5. Relative permittivity profiles reconstructed from noise-free time domain data: (a) first step reconstruction and (b) final reconstruction.

The obtained data were then utilized to reconstruct the dielectric properties by using a nonlinear time domain inversion algorithm. A detailed description of the algorithm can be found in [13]–[14]. It has been shown that permittivity reconstructions have higher quality than conductivity [13]–[14], [34], therefore, we only present the permittivity reconstructions here.

A. Reconstructions from noise-free data

We first reconstruct the image from noise-free data. In the reconstruction, the grid cell size was 2 mm in order to avoid an inverse crime, which happens when the same meshes are used in the forward and inverse simulations, resulting in an unrealistically good reconstruction due to the canceling of numerical errors.

The permittivity reconstructions are shown in Fig. 5 with a reconstruction region of 120 mm $\times$ 120 mm, which is the region surrounded by the dashed rectangular loop in Fig. 4. Fig. 5 (a) gives the first step reconstruction using a spectral content with center frequency 1.5 GHz and bandwidth 1.5 GHz. The objects are found on the correct positions and with dimensions that correspond well to the original model. However, the skin is not well resolved and the reconstructed permittivities of both the skin and tumors are much lower than the real values. The reconstruction was then proceeded using three more steps, where this reconstruction was used as an initial guess. In these three steps of reconstruction, both the center frequency and bandwidth of the used spectral contents were 2 GHz, 2.5 GHz, and 3 GHz respectively. Fig. 5 (b) presents the final reconstruction. Compared with the initial reconstruction in Fig. 5 (a), it is seen that a higher spatial resolution is achieved and the permittivities of the tumors are well consistent with those in the model. The skin is better resolved than the first step reconstruction, but the reconstructed permittivity is still lower than the real value. This is because the thickness of the skin is comparable to the FDTD cell size.

B. Reconstructions from noisy data

Using the same reconstruction settings as for the noise-free reconstruction, we now add different levels of measurement noise to the scattering data. Both the amplitude and phase noise are modeled as zero-mean normal distribution random processes. In order to quantitatively assess the influence of the noise on the reconstructions, a relative reconstruction error is defined:

$$\delta_{rec} = \frac{\iint_S [\epsilon_{rec}^{noisy}(x,y) - \epsilon_{rec}^{noisefree}(x,y)]^2 \cdot ds}{\iint_S [\epsilon_{rec}^{noisefree}(x,y)]^2 \cdot ds}, \qquad (10)$$

where ϵ_{rec}^{noisy} and $\epsilon_{rec}^{noisefree}$ are the permittivity profiles reconstructed from noisy and noise free data. S is the 2-D reconstruction region.

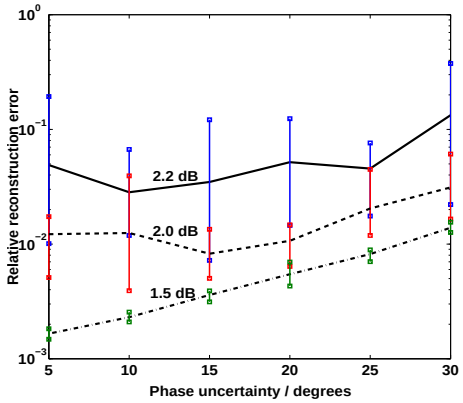

Fig. 6. Relative reconstruction errors when the amplitude and phase errors are taken into account. The dot-dashed line, dashed line and solid line are the average relative reconstruction errors of five repetitive simulations when the amplitude uncertainty is 1.5 dB, 2.0 dB and 2.2 dB respectively. The vertical lines represent the variation ranges of the relative reconstruction errors of the five simulations.

Fig. 6 shows the relative reconstruction errors when different levels of amplitude and phase errors are taken into account. The horizontal axis is the phase uncertainty. The dot-dashed line, dashed line and solid line are the average relative reconstruction errors of five repetitive simulations when the amplitude uncertainty is 1.5 dB, 2.0 dB and 2.2 dB respectively. The vertical lines represent the variations of relative reconstruction errors of the five simulations. It is shown that when the amplitude uncertainty is 1.5 dB, the relative reconstruction error increases with the phase uncertainty and the result varies slightly between individual runs. As the amplitude error increases, the variation of the relative reconstruction error becomes larger.

Fig. 7 presents the reconstructed images with a relative reconstruction error around 0.4%, 0.9%, 4% and 12%. They are obtained for amplitude errors and phase errors of (1.5 dB, 15 degrees), (1.5 dB, 25 degrees), (2 dB, 10 degrees) and (2.2 dB, 15 degrees), respectively. In comparison with the noise free reconstruction in Fig. 5 (b), we can see that a relative reconstruction error less than 0.4% indicates a negligible impact on the reconstruction quality.

V. Conclusion

An analytical analysis has been developed to quantitatively predict the measurement uncertainty of UWB time domain systems due to random errors. The simulations of a specific time domain system confirm the validity of the developed theory.

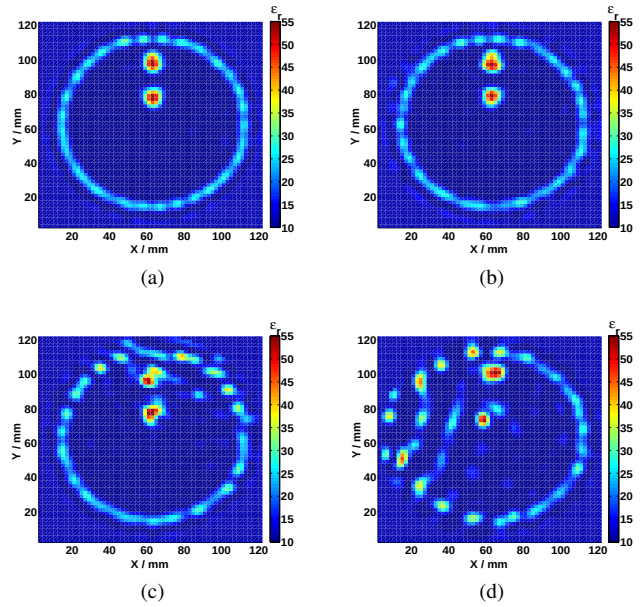

Fig. 7. Reconstructed relative permittivity profiles of the breast model with a relative reconstruction error of (a) 0.4%, (b) 0.9%, (c) 4% and (d) 12%. The corresponding amplitude and phase errors are (a) 1.5 dB, 15 degrees, (b) 1.5 dB, 25 degrees, (c) 2 dB, 10 degrees and (d) 2.2 dB, 15 degrees.

Furthermore, the required measurement accuracy for breast cancer detection has been studied numerically. It is found out that the image distortion is acceptable when the amplitude uncertainty is less than 1.5 dB and the phase uncertainty is less than 15 degrees.

Although the investigation focuses on medical applications of microwave imaging, the analysis can also be applied to other UWB time domain systems.

The study has concentrated on the effects of random errors. As mentioned previously, deterministic errors, although can not be fully compensated for, can be made small by effective calibrations. Another type of error need to be considered in time domain systems is the aliasing error due to inadequate sampling rate. A relevant study carried out by us indicates that the aliasing error is negligible in the frequency range of interest if the time interval resolution is higher than 10 ps.

Future work includes the study of other biological tissue models and the design of a suitable time domain microwave imaging system.

REFERENCES

[1] C. Pichot, L. Jofre, G. Peronnet, and J. C. Bolomey, "Active microwave imaging of inhomogeneous bodies," *IEEE Trans. Antennas Propagat.,* vol. AP-33, no. 4, pp. 416–425, 1985.

[2] P.M. Meaney, M.W. Fanning, D. Li, S.P. Poplack and K.D Paulsen, "A clinical prototype for active microwave imaging of the breast," *IEEE Trans. Microwave Theory Tech.,* vol. 48, no. 11, pp. 1841–1853, 2000.

[3] P. M. Meaney, K. D. Paulsen and John T. Chang, "Near-field microwave imaging of biologically-based materials using a monopole transceiver system," *IEEE Trans. Antennas Propagat.,* vol. 46, no. 1, pp.31–45, 1998.

[4] E. C. Fear, S. C. Hagness, P. M. Meaney, M. Okoniewski and M. A. Stuchly, "Enhancing breast tumor detection with near-field imaging," *Microwave Magazine,* vol. 3, no. 1, pp. 48–56, 2002.

[5] T. S. England and N. A. Sharples, "Dielectric properties of the human body in the microwave region of the spectrum," *Nature*, vol. 163, pp. 487–488, 1949.

[6] A. J. Surowiec, S. S. Stuchly, J. R. Barr, and A. Swarup, "Dielectric properties of breast carcinoma and the surrounding tissues," *IEEE Trans. Biomed. Eng.,* vol. 35, no. 4, pp. 257–263, 1988.

[7] S. Gabriely, R. W. Lau and C. Gabriel, "The dielectric properties of biological tissues: II. Measurements in the frequency range 10 Hz to 20 GHz," *Phys. Med. Biol.,* vol. 41, no. 11, pp.2251–2269, 1996.

[8] M. Lazebnik, D. Popovic, L. McCartney, C. B. Watkins, and etc., "A large scale study of the ultra wideband microwave dielectric properties of normal, benign and malignant breast tissues obtained from cancer surgeries," *Phys. Med. Biol.,* vol. 52, no. 20, pp. 6093–6115, 2007.

[9] S. Y. Semenov, A. E. Bulyshev, A. E. Souvorov, A. G. Nazarov, and etc., "Three-dimensional microwave tomography: Experimental imaging of phantoms and biological objects," *IEEE Trans. Microwave Theory Tech.,* vol. 48, no. 6, pp. 1071–1074, 2000.

[10] W. C. Chew and J. H. Lin, "A frequency-hopping approach for microwave imaging of large inhomogeneous bodies," *IEEE Microwave Guided Wave Lett.*, vol. 5, no. 12, pp. 439–441, 1995.

[11] Q. Fang, P. M. Meaney, and K. D. Paulsen, "Microwave image reconstruction of tissue property dispersion characteristics utilizing multiple-frequency information," *IEEE Trans. Microwave Theory Tech.,* vol. 52, no. 8, pp. 1866–1875, 2004.

[12] F. C. Chen and W. C. Chew, "Time domain ultra-wideband microwave imaging radar system," *J. of Electromagn. Waves and Appl.,* vol. 17, no. 2, pp. 313–331, 2003.

[13] A. Fhager, P. Hashemzadeh, and M. Persson, "Reconstruction quality and spectral content of an electromagnetic time-domain inversion algorithm," *IEEE Trans. Biomed. Eng.,* vol. 53, no. 8, pp. 1594–1604, 2006.

[14] J. E. Johnson, T. Takenaka, and T. Tanaka, "Two-dimensional time-domain inverse scattering for quantitative analysis of breast composition," *IEEE Trans. Biomed. Eng.,* vol. 55, no. 8, pp. 1941–1945, 2008.

[15] E. C. Fear and M. A. Stuchly, "Microwave detection of breast cancer," *IEEE Trans. Microwave Theory Tech.,* vol. 48, no. 11, pp. 1854–1863, 2000.

[16] E. J. Bond, L. Xu, S. C. Hagness and B. D. Van Veen, "Microwave imaging via space-time beamforming for early detection of breast cancer," *IEEE Trans. Antennas Propag.,* vol. 51, no. 8, pp. 1690–1705, 2003.

[17] M. Klemm, I. J. Craddock, J. A. Leendertz, A. Preece and R. Benjamin, "Radar-based breast cancer detection using a hemispherical antenna array-experimental results," *IEEE Trans. Antennas Propagat.,* vol.57, no. 6, pp. 1692–1704, 2009.

[18] S. M. Salvador and G. Vecchi, "Experimental tests of microwave breast cancer detection on phantoms," *IEEE Trans. Antennas Propagat.,* vol. 57, no. 6, pp. 1705–1712, 2009.

[19] J. C. Y. Lai, C. B. Soh, E. Gunawan and K. S. Low, "UWB microwave imaging for breast cancer detection–Experiments with heterogeneous breast phantoms," *Progress in Electromagnetics Research M,* vol. 16, pp. 19–29, 2011.

[20] Y. Yang, C. Zhang and A. E. Fathy, "Development and implementation of ultra-wideband see-through-wall imaging system based on sampling oscilloscope," *IEEE Antennas Wireless propag. Lett.,* vol. 7, pp. 465–468, 2008.

[21] A. G. Yarovoy, T. G. Savelyev, P. J. Aubry, P. E. Lys and L. P. Ligthart, "UWB array-based sensor for near field imaging," *IEEE Trans. Microwave Theory Tech.,* vol. 55, no. 6, pp. 1288–1295, 2007.

[22] W. L. Gans, "Calibration and error analysis of a picosecond pulse waveform measurement system at NBS," *Proceedings of the IEEE,* vol. 74, no. 1, pp. 86–90, 1986.

[23] W. L. Gans, "Dynamic calibration of waveform recorders and oscilloscopes using pulse standards," *IEEE Trans. Instrum. Meas.,* vol. 39, no. 6, pp. 952-957, 1990.

[24] B. N. Taylor and C. E. Kuyatt, "Guidelines for evaluating and expressing the uncertainty Of NIST measurement results," *NIST Technical Note 1297* 1994 Edition.

[25] W. L. Gans, "The measurement and deconvolution of time jitter in equivalent-time waveform samplers," *IEEE Trans. Instrum. Meas.,* vol. IM-32, no. 1, pp. 126–133, 1983.

[26] J. R. Andrews, "Removing jitter from picosecond pulse measurements," *Application Note AN-23,* Picosecond Pulse Labs, Boulder, CO. 2009.

[27] B. Widrow and I. Kollar *Quantization Noise: Roundoff Error in Digital Computation, Signal Processing, Control, and Communications.* Cambridge University Press, Cambridge, UK, 2008.

[28] G. W. Stimson *Introduction to Airborne Radar*, SciTech Publishing, 1998.

[29] Model 3500D Impulse Generator Instruction Manual. *Picosecond Pulse Lab.*

[30] Agilent Technologies Infiniium 90000 X-Series Oscilloscopes (Datasheet) *http://cp.literature.agilent.com/litweb/pdf/5990-5271EN.pdf*
[31] B. Allen, M. Dohler, E. Okon, W. Malik, A. Brown and D. Edwards, *Ultra-Wideband Antennas and Propagation for Communications, Radar and Imaging.* London, U. K.: Wiley, 2006.
[32] A. Shlivinski, E. Heyman, and R. Kastner, "Antenna characterization in the time domain," *IEEE Trans. Antennas Propag.,* vol. 45, no. 7, pp. 1140–1149, 1997.
[33] B. Scheers, M. Acheroy and A. V. Vorst, "Time-domain simulation and characterisation of TEM horns using a normalised impulse response," *IEE Proc.-Microw. Antennas Propag.,* vol. 147, no. 6, pp. 463–468, 2000.
[34] X. Zeng, A. Fhager and M. Persson, "Study on the sensitivity of image reconstruction to the measurement uncertainty in microwave tomography," *The 4th European Conference on Antennas and Propagation.* Barcelona, Spain, 2010.

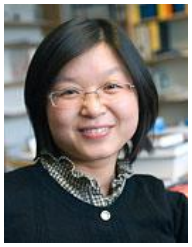

Xuezhi Zeng (S'09) was born in 1980 in China. She received the M.Sc. degree in electrical engineering in 2006 from Jiangsu University, Zhenjiang, China. She is currently working towards the Ph.D. degree at Chalmers University of Technology, Göteborg, Sweden. Her research interests include electromagnetic imaging, antenna design, microwave measurement and system design.

Andreas Fhager (M'07) was born in 1976 in Sweden. He received the M.Sc. degree in engineering physics from Chalmers University of Technology, Göteborg, Sweden in 2001. In 2004 he received the Licentiate of Technology degree in microwave imaging and in 2006 he received the Ph.D. degree in the same field at Chalmers. Currently he is working as an assistant professor at Chalmers. His research interests include electromagnetic imaging methods for breast cancer detection and other biomedical applications of microwaves.

Mikael Persson (M'10) received his MSc and PhD degree from Chalmers University of Technology, Göteborg, Sweden, in 1982 and 1987, respectively. In 2000 he became professor of Electromagnetics and in 2006 Professor in Biomedical Electromagnetics at the Department of Signal and Systems, in Chalmers University of Technology. He is presently the head of the Division of Signal Processing and Biomedical engineering and the director for the regional research and development platform MedTech West. At present these activities involve approximately 50 researchers. His main research interests include electromagnetic diagnostics and treatment. He is author/co-author of more than 200 refereed journal and conference papers.

Peter Linner (S'69-M'74-SM'87-LSM'10) received the M.Sc. and Ph.D. degrees from Chalmers University of Technology, Gothenburg, Sweden, in 1969 and 1974, respectively.

In 1969 he became a Teaching Assistant in mathematics and telecommunications at Chalmers University of Technology. In 1973 he joined the research and teaching staff of the Division of Network Theory at the same university with research interests in the areas of network theory, microwave engineering, and computer-aided design methods. In 1974 he moved to the MI-division, Ericsson Telephone Company, Mölndal, Sweden, where he was a systems engineer and project leader in several military radar projects. He returned to Chalmers University of Technology as a Researcher in the areas of microwave array antenna systems. Since 1981 he has been an Associate Professor in telecommunications. For part of 1992 he spent a period at University of Bochum, Bochum, Germany as a Guest Researcher. His current interest is in the application of computer-aided network methods, microwave circuit technology with emphasis on filters, matching, modeling, and lumped-element methods.

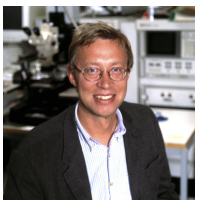

Herbert Zirath (M'80-F'11) received his MSc and PhD degree from Chalmers University of Technology, Göteborg, Sweden, in 1980 and 1986, respectively. He is since 1996 a Professor in High Speed Electronics at the Department of Microtechnology and Nanoscience, MC2, in Chalmers University of Technology. He became the head of the Microwave Electronics Laboratory during 2001. At present he is leading a group of approximately 50 researchers in the area of high frequency semiconductor devices and circuits. His main research interests include foundry related MMIC designs for millimeterwave applications based on both III-V and silicon devices, SiC and GaN based transistors and circuits for high power applications, device modeling including noise and large-signal models for FET and bipolar devices, and InP-HEMT devices and circuits. He is working part-time at Ericsson AB as a microwave circuit expert. He is author/co-author of more than 300 refereed journal/conference papers, and holds 4 patents. He is an IEEE-fellow.